Statistical properties of turbulent bursts in transitional boundary layers

Mark W. Johnson and Ahmad Fashifar
Department of Mechanical Engineering, The University of Liverpool, Liverpool, UK

A digital data acquisition system has been used to collect statistical information of turbulent burst length for a zero-pressure-gradient transitional boundary layer developing on a flat plate with a free-stream turbulence level of 1%. These results are compared with numerical predictions from two turbulent-burst models. The traditional model assumes a constant spot-generation rate, while the new physical model uses a rate proportional to distance from the start of transition. The new model gives a superior prediction of the burst-length statistics that supports the flow physics on which it is based. The results also demonstrate, through the burst length, gap, and spacing distributions, that new spots are not randomly distributed, but are suppressed within a recovery period adjacent to existing spots.

Keywords: transition; transitional boundary layers; intermittency; turbulent spots

Introduction

Much research is currently in progress into providing accurate boundary-layer transition prediction. These predictions are primarily for use in C.F.D. codes for geometries such as gas turbine blades or aircraft wings, where the transitional boundary layer covers a significant proportion of the wetted surface. Currently, prediction relies heavily on empirical correlations for flat plates (e.g., Abu Ghannam and Shaw 1980), but few data are available for common practical geometries including features such as blade curvature and sweep. A fuller understanding of the physics for transitional flow is therefore desirable so that the effects of geometry can be more reliably anticipated.

Direct Numerical Simulation has been successful in accurately predicting transition on flat plates (see Savill 1991) and hence presumably in modeling the flow physics. Detailed analysis of burst formation and development within these numerical models may well improve the understanding of transition in the future. Digital signal processing and conditional sampling techniques have also advanced experimental methods enormously over the last decade. This advance not only has led to the development of reliable intermittency measurement techniques but also permits the separate analysis of the turbulent and laminar periods (Kuan and Wang 1989; Blair 1992; Fashifar and Johnson 1992). The objective of the current work was to use such experimental techniques to provide statistical information on turbulent bursts and to compare the results with the predictions from two transition models.

Address reprint requests to Dr. Johnson at the Department of Mechanical Engineering, The University of Liverpool, P.O. Box 147, Liverpool L69 3BX, UK.

Received 19 July 1993; accepted 13 December 1993

Experimental arrangement

A boundary-layer suction wind tunnel, described by Fashifar (1992) and Fashifar and Johnson (1992), was used for the measurements. The flat plate has an elliptical leading edge, is 1219 mm long and 718 mm wide, and is inclined at 0.5° to the flow such that the stagnation point is located on the upper surface of the plate very close to the leading edge. In the current work, a turbulence-generating grid is placed 0.75 m upstream of the plate leading edge such that the freestream turbulence level is close to 1% at all the measurement locations. The upper flexible wall is adjusted to provide a zero pressure gradient on the plate. All boundary-layer measurements were made using a Dantec boundary-layer probe connected to a Dantec C system anemometer that was interfaced through a 12-bit a-d converter to a PC. The hot-wire signal is digitized at a sampling rate of 10 kHz and then linearized by means of a look-up calibration table. A full description of this procedure and hot-wire calibration is given in Fashifar (1992).

The algorithm for laminar/turbulent discrimination is described in detail in Fashifar and Johnson (1992). The hot wire is placed close to the plate surface ($y/\delta \cong 0.1$). The digitized signal is linearized and then filtered using a Butterworth high-pass filter with a cutoff frequency of $U/2\pi\delta$ Hz, where U is the free-stream velocity and δ the boundary-layer thickness. This frequency corresponds approximately to the frequency of the largest turbulent vortices that can be accommodated in the boundary layer, and hence low frequencies removed by the filter are due to laminar instability waves or fluctuations convected from the free stream. A window is now placed around the filtered signal, and those portions outside the window are deemed turbulent. In addition, where the signal is only resident within the window briefly (less than $2\pi\delta/U$ seconds), it is also considered to be part of the turbulent-burst signal. The window size that gave most reliable results was established empirically as 10% of local velocity.

All the measurements presented were taken with a free-stream velocity of 13.8 m/s at five different chordwise positions within the transitional boundary layer, where the

intermittency γ equals 0.1, 0.25, 0.5, 0.7, and 0.9. The start and end time of each of approximately 20,000 turbulent bursts was recorded at each of these chordwise locations, from which distributions of burst length, gap length, and burst spacing were determined.

Burst models

Two models are used to predict burst properties through transition. The first or traditional model (Dhawan and Narasimha 1958) assumes that all the spots are initiated at the start of transition location and then grow at a constant rate in the streamwise x and spanwise z directions as they travel downstream. Turbulent intermittency is defined as the proportion of time at which the flow is turbulent at a fixed point in space. Here it is clearer to use an alternative but equivalent definition. For a two-dimensional (2-D) boundary layer, the intermittency is the proportion of a spanwise line occupied by turbulent flow at a fixed instant of time. Using this definition, it follows that, if the spots propagate at a rate σ,

$$\frac{d\gamma}{dx} = N\sigma \tag{1}$$

where N is the number of spots present per unit length of the line.

The spots are initiated at the start of transition position at a rate of n per unit span per unit time and therefore reach the spanwise line at the same rate. However, some of the spots merge with neighboring spots at a rate of $\gamma n/U_S$ prior to reaching this line. In addition, the turbulent regions on the line will grow and merge with neighboring regions at a rate of $N^2\sigma/(1-\gamma)$. Thus the overall rate of appearance of spots is

$$\frac{dN}{dx} = \frac{(1-\gamma)n}{U_S} - \frac{N^2\sigma}{(1-\gamma)} \tag{2}$$

Combining Equations 1 and 2,

$$(1-\gamma)\frac{d^2\gamma}{dx^2} + \left(\frac{d\gamma}{dx}\right)^2 - \frac{\sigma n}{U_S}(1-\gamma)^2 = 0 \tag{3}$$

Assuming $\sigma n/U_S$ is constant,

$$\gamma = 1 - \exp\left(-\frac{\sigma n}{2U_S}(x - x_S)^2\right) \tag{4}$$

or

$$\gamma = 1 - \exp(-0.412\zeta^2) \tag{5}$$

where $\zeta = (x_S - x_{0.25})/(x_{0.75} - x_{0.25})$ is the Narasimha dimensionless length parameter. It follows that the burst observance rate is given by

$$N/N_{max} = 1.5(1-\gamma)\zeta \tag{6}$$

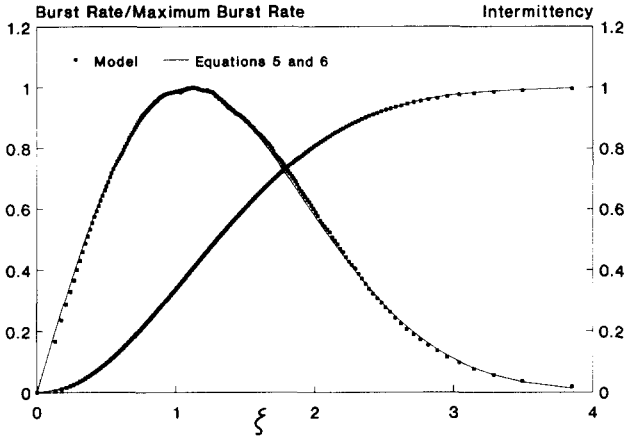

Figure 1 Comparison of analytical and numerical results for traditional burst model

The model was implemented on a computer by considering a spanwise line, of unit length, as it travels downstream at the spot velocity U_S. Spots are generated at random positions on this line at a constant rate of n spots per unit time per unit span and are allowed to grow in the spanwise direction at a constant rate of σ units span per unit length traveled in the streamwise direction. New spots are initiated by a random-number generator only when this leads to a spot position within a laminar region. In addition when the gap reduces to zero between any two adjacent spots due to their growth, they merge and are subsequently considered as a single spot.

Values of U_S, σ, and n are chosen in order to provide a sufficiently large number of turbulent bursts (over 500,000) for statistical analysis. The intermittency values should be independent of $\sigma n/U_S$, as shown by Equation 5. The code is therefore verified by comparing the computational results for intermittency and burst rate with the analytical values given by Equations 5 and 6. As shown in Figure 1, a very close correlation clearly exists between the numerical and analytical results, which is taken as confirmation that no significant changes would occur if a larger number of bursts had been considered.

The second, new model is based on the physical start of the transition criterion formulated by Johnson. Johnson (1993) used physical arguments to demonstrate that when the instantaneous velocity close to the wall drops to 50% of the

Notation

l	Burst length
$\bar{l}$	Mean burst length
n	Spot rate per second per meter span
N	Number of bursts per meter span
r	Recovery length
t	Time
U	Free-stream velocity
U_S	Spot velocity
x	Streamwise distance along plate
x_S	Start of transition position on plate
$x_{0.25}, x_{0.75}$	$\gamma = 0.25$ and 0.75 positions on plate

Greek symbols

α	Constant in Equation 11
γ	Intermittency
δ	Boundary-layer thickness
σ	Spot growth rate
ξ	$= (x - x_S)/(x_{0.75} - x_{0.25})$ - Narasimha transition length
ζ	The Narasimha dimensionless length parameter, $(x_S - x_{0.25})/(x_{0.75} - x_{0.25})$

local mean velocity, a turbulent spot will be generated. Now, assume that the near wall velocity signal can be approximated by the isotropic power spectrum used by Hinze (1959), i.e.,

$$\frac{4u'^2 l}{EU} = 1 + \left(\frac{2\pi f l}{u}\right)^2 \tag{7}$$

where E is the power spectral density, f is the turbulent frequency, u'^2 is the turbulent kinetic energy, and l is the integral length scale. If such a signal (Figure 2) is analyzed, the distribution of velocity "trough" depths is as shown in Figure 3.

For levels of $u'_b/u'_{rms} > 1.2$, this proportion can be represented by

$$P = \frac{u'_{rms}/u'_b - 0.4}{1.6} \tag{8}$$

Now using Johnson's criterion that $u'_b = u/2$ for spot initiation,

$$P = \frac{u'_{rms}/u - 0.2}{0.8} \tag{9}$$

Johnson (1993) also provides an empirical correlation for the growth of the fluctuations close to the wall, namely,

$$\frac{uu'_{rms}}{U^2} = \beta \mathrm{Re}_\delta^2 Tu \left(\frac{y}{\delta}\right)^2 \tag{10}$$

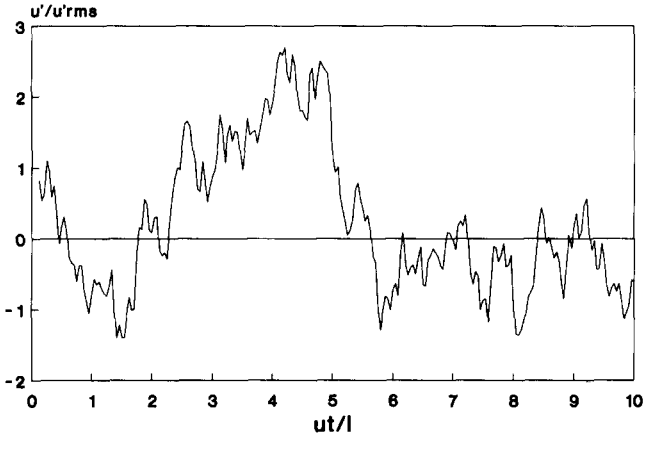

Figure 2 Isotropic turbulent signal

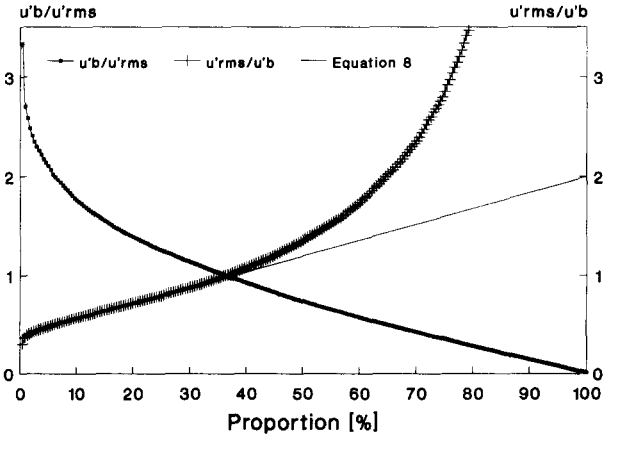

Figure 3 Depth of spots producing troughs in an isotropic turbulent signal

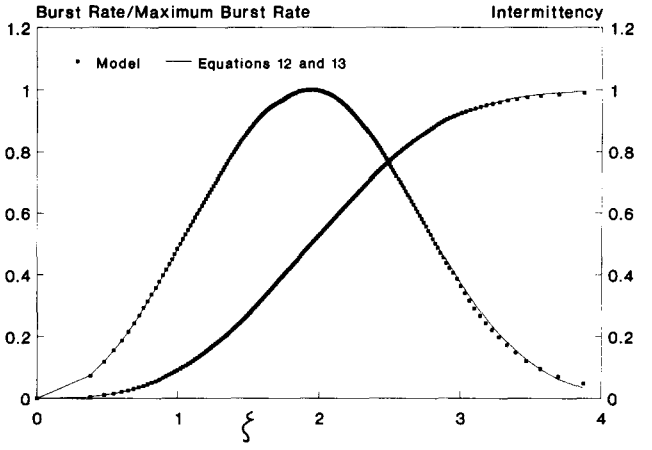

Figure 4 Comparison of analytical and numerical results for new physical burst model

where β is a constant that depends on the free-stream turbulent level. For a flat-plate laminar boundary layer, Re_δ^2 is proportional to Re_x, and Equations 9 and 10 indicate that the number of spot-inducing troughs will increase linearly with downstream distance. Therefore, in the new model,

$$\frac{\sigma n}{U_S} = \alpha(x - x_s) \tag{11}$$

where α is a constant. This leads to the algebraic relationships

$$\gamma = 1 - \exp(-0.0941\ \zeta^3) \tag{12}$$

and

$$\frac{N}{N_{max}} = 0.528(1 - \gamma)\zeta^2 \tag{13}$$

Again, the numerical results with a maximum of over 500,000 bursts closely resemble the algebraic values, as shown in Figure 4.

Burst length

The experimental results for burst lengths at $\gamma = 0.1$, 0.25, 0.5, 0.7, and 0.9 are presented as histograms in Figures 5a to 5e, respectively. The distributions appear similar through transition, but small differences do exist, as shown when the distributions are compared in Figure 6. At low intermittencies, the average gap between bursts is large, and hence the number of mergings between bursts is small. It therefore follows that the probability of very long bursts due to one or more mergings of shorter bursts is very low, with only 4% of the turbulent period consisting of bursts that are more than four times the average burst length at $\gamma = 0.1$. As the intermittency increases, mergings become more frequent, and hence there is an increase in the proportion of long bursts with a compensating decrease in shorter bursts, as shown in Figure 6.

The results from the traditional model (Figure 7) differ significantly from the experimental distributions and also show a greater variation with intermittency. At $\gamma = 0.1$, a rapid decrease exists for the model distribution for the number of bursts longer than $1.5\,\bar{l}$. This is because the constant spot-generation rate assumed in the model will lead to, prior to any merging, an equal number of bursts in each band and to the "no merging" distribution shown in Figure 7. The small number of bursts longer than the $1.5\,\bar{l}$ critical length therefore result from the merging of shorter bursts. Since the

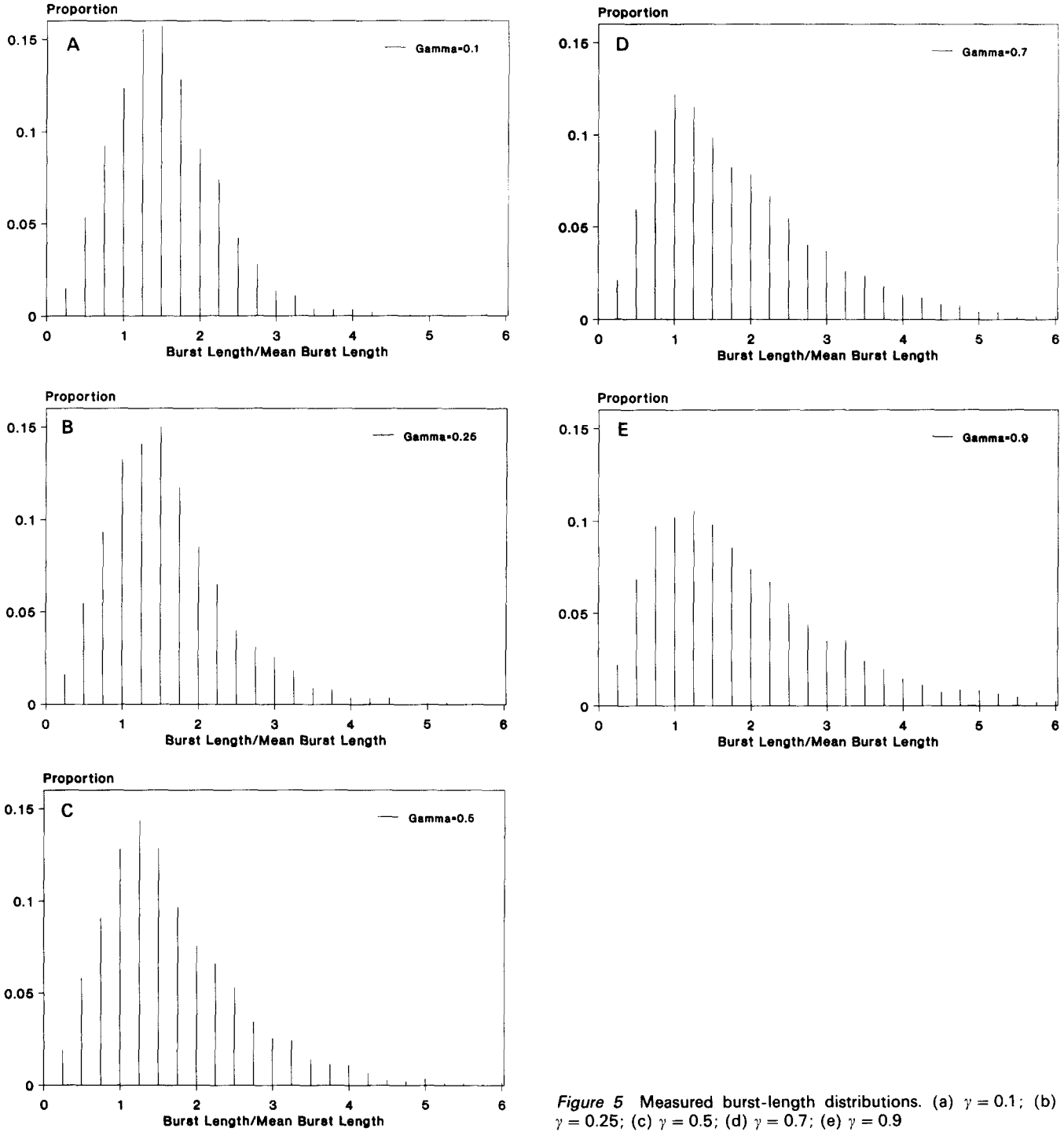

Figure 5 Measured burst-length distributions. (a) $\gamma = 0.1$; (b) $\gamma = 0.25$; (c) $\gamma = 0.5$; (d) $\gamma = 0.7$; (e) $\gamma = 0.9$

experimental results in Figure 5a do not exhibit this rapid decrease, it can be concluded that the assumption of a constant spot-generation rate is invalid. As the intermittency increases, this feature in the model distribution becomes less significant, although it is still apparent up to $\gamma = 0.5$. It is only finally erradicated once sufficient merging of the early bursts has occurred. Thus the model results at $\gamma = 0.7$ and $\gamma = 0.9$ are fairly similar to the experimental distributions.

The new-model results bear a much closer resemblance to the experimental distribution, as shown in Figure 8. In this case, the spot-production rate is proportional to the distance from the start of transition; hence, for low intermittency where no merging has occurred, only a few long bursts are present, as shown by the parabolic "no merging" distribution in Figure 8. A trend similar to that of the experimental results is observed as the intermittency increases, with an increase in the proportion of long bursts and a decrease in short bursts. If the distributions at $\gamma = 0.1$ are compared in Figures 5 and 8, however, it can be seen that the model predicts a lower proportion of bursts with a length less than $2\bar{l}$ and a slightly larger number of long bursts than were observed experimentally. This prediction is believed to be because merging of bursts

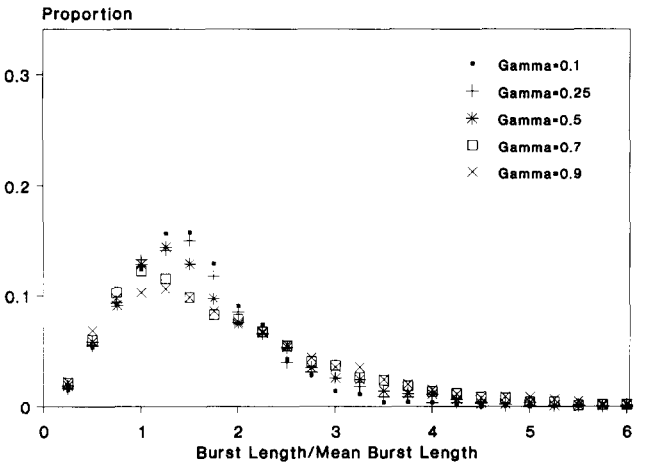

Figure 6 Comparison of measured burst-length distributions. Band width = 0.25

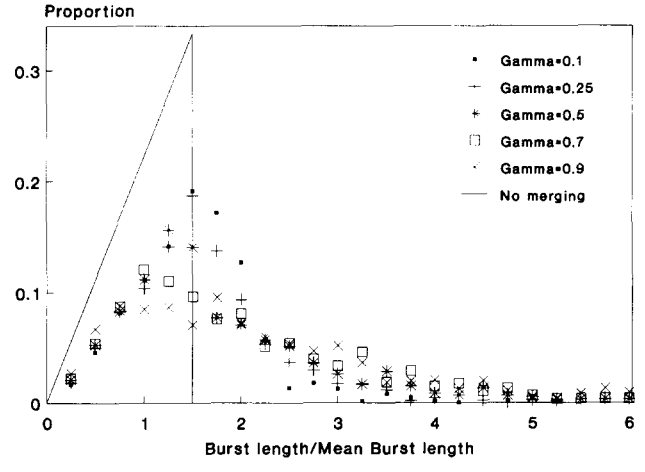

Figure 7 Predicted burst-length distributions using the traditional model. Band width = 0.25

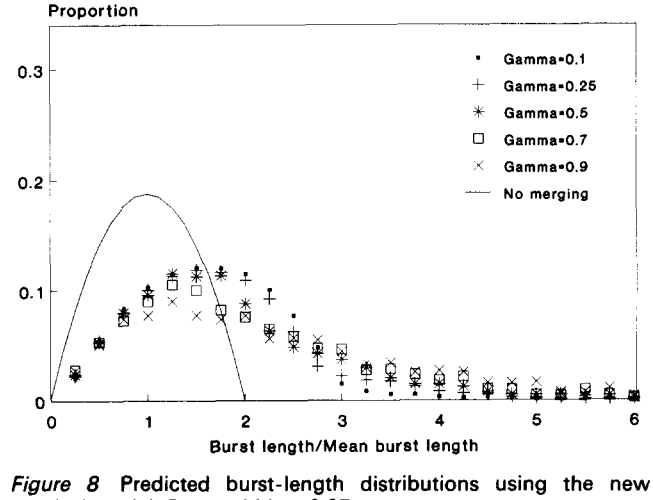

Figure 8 Predicted burst-length distributions using the new physical model. Band width = 0.25

is less probable at low intermittencies than the model suggests. This implies that spot-initiation locations are not truly random, but tend to be least likely to be close to existing spots, which would lead to early merging, and more likely to be distant from existing spots, which would delay merging. This in turn may be due to the fact that the troughs in the turbulent viscosity signal, which initiate the spots, are not randomly distributed. Alternatively, the increased mean velocity in the recovery period following each turbulent spot may suppress further spot initiation, such that new spots only form some distance from existing spots.

Gap length

The measured and the two model gap-length distributions are shown in Figures 9, 10, and 11, respectively. The distribution of gaps at an intermittency γ is seen to be almost identical to the burst-length distribution at an intermittency $1-\gamma$. This suggests that the process of shrinkage and disappearance of the gaps mimics the appearance and growth of bursts. The experimental gap length at $\gamma = 0.9$ (Figure 9) shows a greater uniformity of size than either model (Figures 10 and 11), suggesting that the gaps are not randomly distributed, but like the bursts, tend to a rather more equal spacing.

Burst spacing

The spacing is defined here as the distance between the centers of consecutive bursts. The experimental spacing distributions,

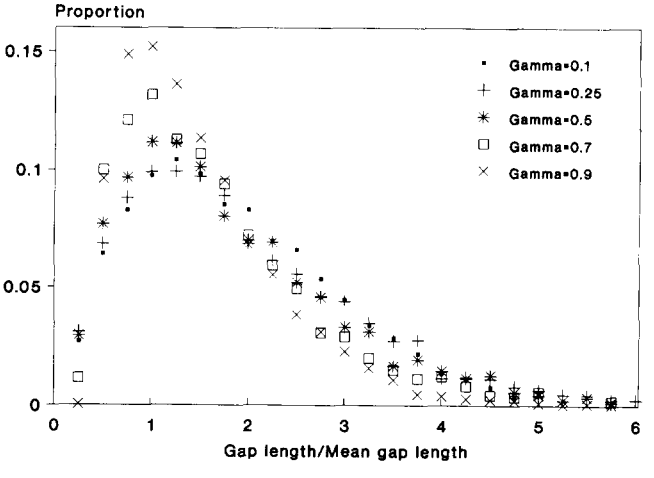

Figure 9 Measured gap-length distributions using the traditional model. Band width = 0.25

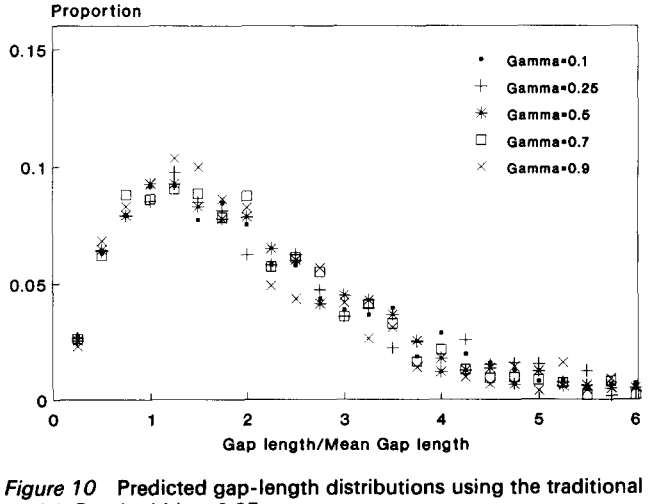

Figure 10 Predicted gap-length distributions using the traditional model. Band width = 0.25

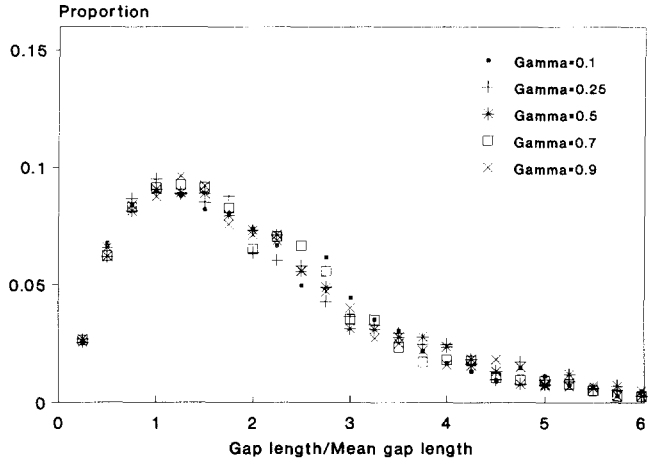

Figure 11 Predicted gap-length distributions using the new physical model. Band width = 0.25

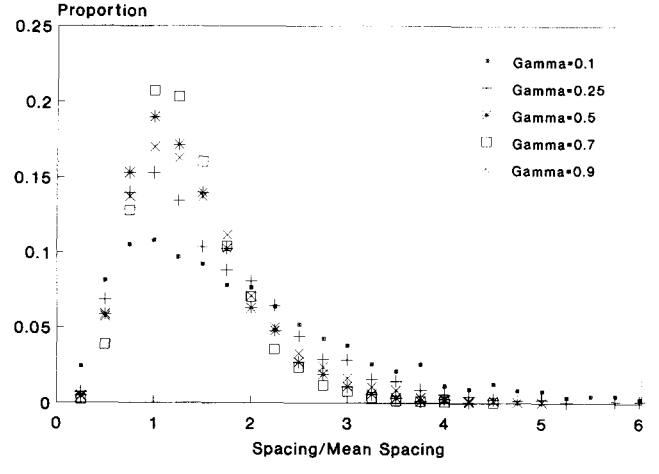

Figure 12 Measured burst-spacing distributions. Band width = 0.25

shown in Figure 12, indicate that the most probable spacing is close to the mean at all intermittencies. This mean spacing becomes more probable as the intermittency increases up to $\gamma = 0.7$, but it decreases once again for higher intermittencies. At low intermittency, the burst spacing is large and varies in length considerably, with significant number of spacings 4 or 5 times the average length. However, long gaps between bursts are more likely to be divided by new spots than shorter gaps, and hence the range of spacings narrows until at $\gamma = 0.7$ a negligible number of spacings exist that are greater than four times the average. For $\gamma > 0.7$, the intermittency increases, not so much due to the formation of new spots but rather due to the growth of existing ones. Since all the spots grow at the same rate, spots that are close together will tend to merge more frequently than those spaced far apart. Therefore, a decrease in the proportion of spacings less than about 1.5 times the average is observed between $\gamma = 0.7$ and 0.9, with a compensatory increase in the proportion of longer spacings.

Figure 13 shows the predicted burst spacing using the Dhawan and Narasimha model. The experimental distribution at $\gamma = 0.1$ is well predicted, which suggests that the spots are randomly distributed; however, since only a small number of widely spaced bursts exist, the effect of suppression of spot initiation in the recovery period following each spot will be negligible. As the intermittency increases, the predictions deviate more from the experimental observations. The measurements indicate a rather more regular distribution (i.e., a higher proportion of spacings close to the mean) than the prediction. This result is probably due to suppression of the spot initiation in the recovery period, which has a more significant effect as the number of bursts and hence the proportion of the signal occupied by the recovery periods increases. For $\gamma = 0.7$, the predicted distribution widens again, as observed experimentally, and is due to the more frequent disappearance of short spacings due to burst growth and merging.

The new-model burst-spacing distribution predictions are shown in Figure 14. These are very similar to the traditional model results, with good prediction of the experimental distribution at low intermittency but with a wider predicted distribution for intermediate and high intermittencies. Differences between the two model predictions are due to the fact that for intermittencies up to 0.4, the number of bursts is lower in the new model. This results in fewer mergings and hence a slightly narrower distribution of spacings, which provides a slightly improved prediction of the experimental observations.

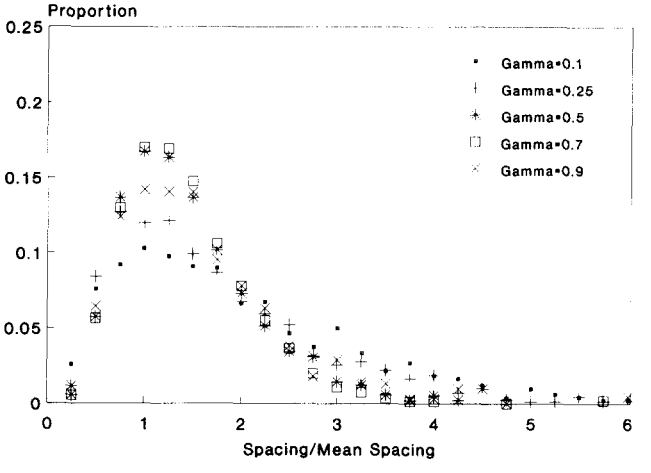

Figure 13 Predicted burst-spacing distributions using the traditional model. Band width = 0.25

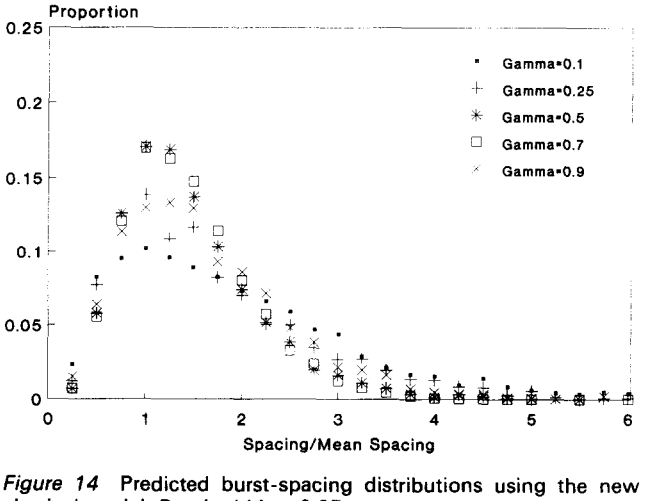

Figure 14 Predicted burst-spacing distributions using the new physical model. Band width = 0.25

Recovery-length model

The reason postulated for differences between the new model and measured distributions is that spot formulation is suppressed within a recovery length following each existing spot. In order to test this postulate, the new model was modified to incorporate this effect, with new spots suppressed for spanwise distance r adjacent to existing spots where $r(\alpha/\sigma^2)^{1/3} = 0.014$. Algebraic expressions for intermittency γ and burst rate N cannot be determined, and so the model results are compared with the zero-recovery-length expressions (Equations 12 and 13) in Figure 15. At intermittencies below 0.35, the number of bursts is reduced, but above this value, fewer burst mergings occur because of the more regular burst spacing. For $\gamma > 0.5$, the recovery periods occupy a significant proportion of the signal, and the resulting suppressions of new spots leads to a lower burst rate. Once $\gamma = 0.9$ is reached, the recovery periods virtually suppress all new spots, and therefore the increase in intermittency is due almost entirely to spot growth. Consequently, the intermittency approaches unity more slowly than Equation 12 implies.

Figures 16, 17, and 18 show the modified burst length, gap, and spacing distributions, respectively. The effect of including recovery period is to narrow the distribution and to increase the height of the peak, which leads to predictions much closer to the corresponding measured distributions (see Figures 6, 9, and 12).

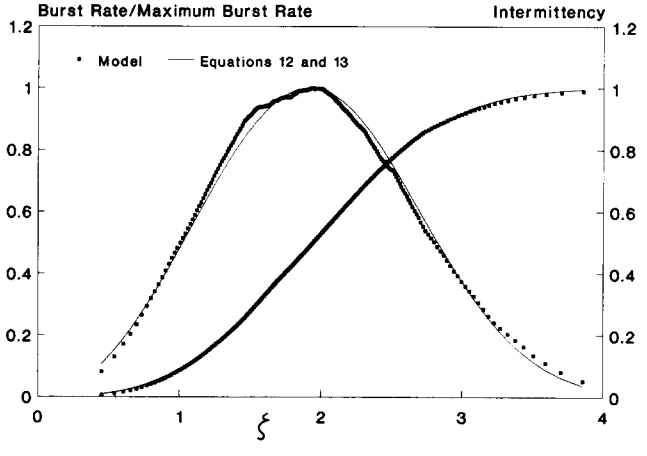

Figure 15 Comparison of the numerical results for the recovery-length model with the analytical results with no recovery length

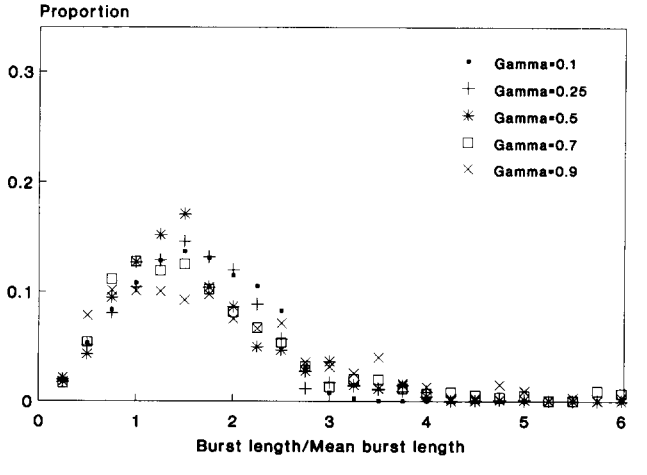

Figure 16 Predicted burst-length distributions using the recovery-length model. Band width = 0.25

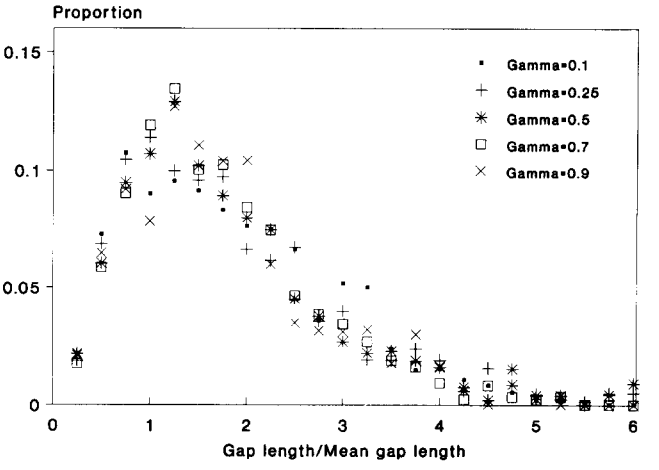

Figure 17 Predicted gap-length distributions using the recovery-length model. Band width = 0.25

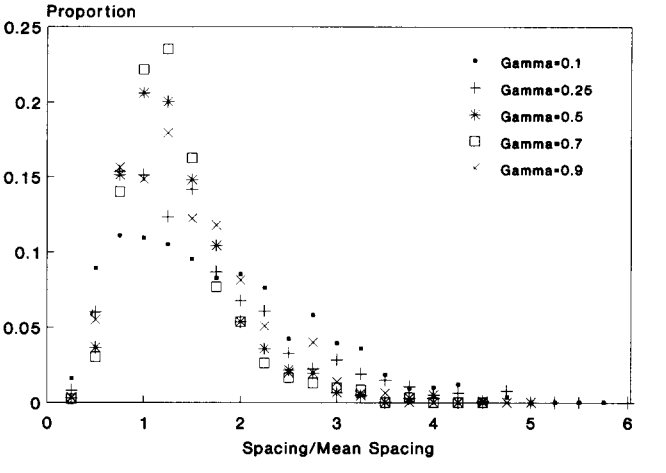

Figure 18 Predicted burst-spacing distributions using the recovery-length model. Band width = 0.25

Conclusions

(1) Burst-length distributions are similar through transition, but more bursts merge as the intermittency increases, resulting in a decrease in the proportion of short bursts with a compensatory increase in the proportion of longer bursts.

(2) The physical model formulated by Johnson (1993) gives a better prediction of burst- and gap-length distributions than the traditional Dhawan and Narasimha (1958) model.

(3) The random spot-initiation position used in the models does not accurately predict experimental burst length at low intermittencies or burst spacing at intermediate and high intermittencies. However, when spot initiation is suppressed within the recovery period following each turbulent burst, good prediction of burst, gap, and spacing distributions is obtained.

References

Abu Ghannam, B. J. and Shaw, R. 1980. Natural transition of boundary layers—the effect of turbulence, pressure gradient and flow history. *J. Mech. Eng. Sci.*, **22** (5), 213

Blair, M. F. 1992. Boundary layer transition in accelerating flows with intense freestream turbulence, Parts 1 and 2. *ASME J. Fluids Eng.*, **114**, 313–332

Dhawan, S. and Narasimha, R. 1958. Some properties of boundary layer flow during the transition from laminar to turbulent motion. *J. Fluid Mech.*, **3**, 418

Fashifar, A. 1992. Mechanisms of boundary layer transition. Ph.D. thesis, Dept. of Mechanical Engineering, University of Liverpool, Liverpool, United Kingdom

Fashifar, A. and Johnson, M. W. 1992. An improved boundary layer transition correlation. ASME paper 92-GT-245. Presented at the Gas Turbine Congress, Cologne, June 1992

Hinze, J. O. 1959. *Turbulence — Introduction to its Mechanism and Theory*. McGraw-Hill, New York

Johnson, M. W. 1993. A bypass transition model for boundary layers. Paper no. 93-GT-90, presented at the ASME Gas Turbine Congress, Cincinnati, May 1993. To be published in *ASME J. Turbomachinery*

Kuan, C. and Wang, T. 1989. Some intermittent behaviour of transitional boundary layer. *Proc. AIAA 20th Fluid Dyn. Plasma Dyn. Lasers Conf.*, Paper no. AIAA 89-1890, AIAA, Buffalo, NY, June 1989

Savill, A. M. 1991. A synthesis of T3 test case predictions. *Proc. 1st ERCOFTAC Workshop*. Cambridge University Press, Cambridge, UK